Soft Matter

Cite this: *Soft Matter*, 2012, **8**, 11173

www.rsc.org/softmatter

PAPER

The effect of depletion layer on diffusion of nanoparticles in solutions of flexible and polydisperse polymers

Anna Ochab-Marcinek,[a] Stefan A. Wieczorek,[a] Natalia Ziębacz[a] and Robert Hołyst*[ab]

Received 20th April 2012, Accepted 10th July 2012
DOI: 10.1039/c2sm25925g

We introduce a model of diffusion of nanoparticles in solutions of flexible, polydisperse polymers. The model takes into account the effect of depletion layer with soft boundaries. The presence of depletion layer leads to nonlinear dependence of the mean square displacement (MSD) on time. Our model may be an alternative choice for the study of those experimental systems where the crossover between subdiffusion and normal diffusion is observed. Its advantage is mathematical simplicity: it allows easy identification of the crossover times and distances, which are here associated with the depletion layer thickness. The soft boundaries of the depletion layer, generated by the flexible and polydisperse polymers, are here approximated by two shells enclosed one in another, which may be interpreted as approximations of polymer density profiles around the probe. We show a very good agreement of the model with dynamic light scattering (DLS) measurements of diffusion of nanoparticles in solutions of polyethylene glycol (PEG).

1 Introduction

Diffusion in a crowded environment is often described in terms of anomalous diffusion,[1–10] a process where the mean square displacement (MSD) of the probe depends on time as $\langle r^2(t)\rangle \sim t^{\alpha}$, $\alpha \neq 1$. Such studies mainly focus on finding the values of the anomalous exponent α for a given experimental system. The shortcoming of this approach is that the knowledge of the value of α does not provide any information about the physical properties of the system, except for the notion that $\alpha < 1$ indicates diffusion hindered by some factors and $\alpha > 1$ is the signature of facilitated diffusion.

In the recent paper,[11] Sokolov broadly reviews the uses of anomalous diffusion models in soft matter research. There are a number of such theoretical models: in trap models,[12] anomalous diffusion is caused by the assumption that the particles are geometrically or chemically trapped for some time during their diffusive motion, and the probability density function of the waiting times is a power-law distribution. Geometric trapping that can be described by such models was found in the transport of particles in Purkinje cells, where dendritic spines played the role of traps.[13,14] Chemical trapping by nonspecific binding to DNA was proposed by Saxton[15] as an explanation for anomalous diffusion of Cajal bodies in the cell nucleus.[16] Models of Levy flights simply assume that the spatial increments in object's motion are drawn from a heavy-tailed probability distribution. In the theoretical work by Metzler *et al.*,[17] studying the role of DNA conformation in protein sliding, the simulated DNA loop sizes were found to have power-law distributions, and thus the jumps between knotted DNA segments were Levy flights. A similar effect of jumping was found in experiments,[18] although it was not interpreted in terms of Levy flights. The models of motion in labyrinthine environments, such as percolation models, assume that the geometry of the medium is fractal. Höfling *et al.*[19] proposes that the anomalous diffusion of GFP in the cell membrane[20] can be described by a percolation model. In viscoelastic models,[21] the memory kernel is assumed to have a power-law form. In the experimental tracking of probe motion during protein layer formation at an oil–water interface,[22] the non-linear MSD was interpreted as a result of viscoelastic interactions. Scaled Brownian motion[23] is a model where the diffusion coefficient is assumed to depend on time in a power-law manner. This type of model was used to interpret the experiments on motion of colloidal particles in a modulated potential generated by a laser beam.[24]

Therefore, anomalous diffusion in polymer fluids is a well-established and quantified fact. As with all theoretical models, this type of description requires certain assumptions (that the probability distribution of waiting times is heavy-tailed, or the diffusion equation is fractional, or the memory kernel of a viscoelastic system has a power-law dependence on time, or the diffusion coefficient depends on time in a power-law manner, or the medium geometry is fractal, *etc.*). Anomalous diffusion is also used in the bottom-up approach, where one solves a model that does not contain assumptions of anomalousness, but the power law turns out to be a handy approximation of the solution (*e.g.* as in the Rouse and reptation models[25]). In such models the

[a]*Institute of Physical Chemistry, Polish Academy of Sciences, ul. Kasprzaka 44/52, 01-224 Warsaw, Poland. E-mail: holyst@ichf.edu.pl*
[b]*Cardinal Stefan Wyszyński University, WMP-SNŚ, ul. Dewajtis 5, 01-805 Warsaw, Poland*

anomalous exponent varies depending on the time scale of the measurement. Crossover to free diffusion has been observed experimentally in the limits of very short as well as very long time scales.[1–5] However, not much attention has been paid to date to identification of the sources of the anomalous behavior and the crossover time scales in those systems.[6] Within the framework of anomalous diffusion, this problem was not widely investigated theoretically due to mathematical complexity of the description. Nevertheless, there exist successful approaches in terms of percolation models.[7,8]

We propose a model that may be an alternative choice for the study of those experimental systems where the crossover between hindered diffusion and normal diffusion is observed. In our previous paper,[26] we proposed that the effect of depletion layer can be the cause of the nonlinearity of MSD of objects diffusing in complex liquids. We have shown that this nonlinear behavior can be approximated by anomalous diffusion with α varying depending on the measurement time scale and tending to 1 in both short and long time scales. The model of walking confined diffusion that we introduced to describe this effect requires different assumptions than the anomalous diffusion model: the geometry of the confinement experienced by the diffusing probe (the depletion layer) is not fractal but spherical, and the confinement diffuses itself, independently of the diffusion of the probe. The model also assumes a mathematical approximation which reduces the formula for MSD to a simple exponential form. The advantage of our model is its mathematical simplicity: it allows easy identification of the crossover times and distances, which are here associated with the depletion layer thickness.

The depletion layer[27,28] is an exclusion zone that forms around a particle immersed in a solution of non-adsorbing polymer. The effect occurs due to the changes of configurational entropy of polymer chains:[29] close to the particle surface, the entropy strongly decreases because of chain deformation, so that the centres of masses of polymer chains are excluded from that region. This results in a polymer concentration gradient across the depletion layer boundary. Theoretical studies[30] suggest that the thickness of the depletion layer should decrease with increasing polymer concentration. At the overlap concentration it should be comparable to the radius of gyration R_g of the polymer.

The model of walking confined diffusion that we introduced in the previous study[26] approximated the depletion layer as a single shell with a reflecting boundary, filled with a medium of viscosity lower than the bulk. The MSD of a diffusing particle was then given by the formula:

$$\langle \boldsymbol{r}^2(t) \rangle = 6D_L t + \frac{6}{5}\delta^2\left(1 - e^{-\frac{5D_S t}{\delta^2}}\right), \qquad (1)$$

where t is the time, D_L is the long-time diffusion coefficient, D_S is the short-time diffusion coefficient, and δ is the depletion layer thickness. The single-shell model (1) fitted very well the literature data on solutions of rigid and monodisperse polymers (fd-viruses). It also fitted well the literature data on rigid but polydisperse polymers (F-actin, F-actin + scruin). The model was successful in these cases probably because the rod-like molecules could form a rigid cage around the probe, in agreement with the model's assumption of reflecting boundary conditions.

However, the single-shell model did not fit well the literature data on the MSD of probes in solutions of a flexible and polydisperse polymer (polyethylene oxide), where the presence of long but flexible polymer chains and also short, faster-diffusing chains softened the boundary of the depletion layer. Moreover, we found inconsistencies between the data obtained in different experiments with rigid polydisperse polymers (F-actin), which suggested that these experiments might have been carried out under poorly controlled conditions. These observations clearly indicated the need for new, well-controlled experiments with flexible and polydisperse polymers, as well as the need for development of an improved model that would fit the mean square displacement for such systems.

We address this problem in the present study. The goal is to provide the model of diffusion of nanoparticles in solutions of flexible and polydisperse polymers, such that it would (differently from the anomalous diffusion models) be able to cover the crossover timescales, and, explicitly taking into account the physical causes of the "anomalous" behavior, it would be able to give quantitative information about the thickness of the depletion layer and the structure of its boundaries. The proposed model is presented in Section 2.

According to the theoretical predictions,[30] the depletion layer thickness δ should be the largest when the probe radius R is comparable to the radius of gyration R_g of the polymer. Therefore, to validate the theoretical predictions, we carried out dynamic light scattering (DLS) experiments with probes of the radius $R = 20$ nm in the solutions of PEG 600K ($R/R_g = 0.65$), $R = 20$ nm in the solutions of PEG 2M ($R/R_g = 0.45$), and $R = 43.5$ nm in the solutions of PEG 2M ($R/R_g = 0.98$). Both polymers were strongly polydisperse: their molecular masses varied by over 2 orders of magnitude (see Table 1, Fig. 2 and ref. 31). Section 3 describes the details of the experimental setup and in Section 4 we present the results of fitting the theory to the experimental data.

2 Model

Although the single-shell model (1) turned out to be insufficient for solutions of flexible, polydisperse polymers,[26] the model of depletion layer as a perfectly reflecting sphere is compelling due to the simplicity of the calculation of MSD. Therefore, in the present study we propose the double-shell model (Fig. 1) as an empirical extension of the result of the earlier theory for rigid polymer, and as a tool to fit experimental data, which can better approximate the soft boundaries of the depletion layer but it is still extremely easy to treat mathematically.

We assume that the depletion layer consists of two reflecting spheres, enclosed one in another. Enclosed in the inner sphere is

Table 1 Parameters of the polyethylene glycol (PEG) used in the experiments. See also Fig. 2 for the distribution of molecular masses for the commercially purchased PEGs

	PEG 600K	PEG 2M
Number average molecular masses, M_n [Da]	276 862	521 563
Polydispersity index PDI	2.81	2.13
Radius of gyration, R_g [nm]	30.83	44.51
Overlap concentration, c^* [%]	0.37	0.23
Concentration range [%]	0.5–2	0.3–1.5

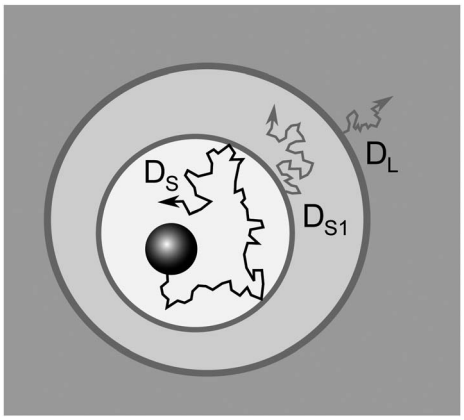

Fig. 1 Double-shell model of depletion layer. To model the soft boundary, we assume that the depletion layer consists of two reflecting spheres, enclosed one in another. Enclosed in the inner sphere is the probe of the radius R. The probe, the inner layer and the outer layer diffuse independently with the diffusion coefficients $D_S > D_{S1} > D_L$.

the probe of the radius R. The probe moves inside the inner sphere with the short-time diffusion coefficient D_S. The inner sphere (of the radius $R + d$) moves together with the probe with the intermediate diffusion coefficient D_{S1}. The outer sphere (of the radius $R + d_1 + d$) moves diffusively together with its content, with the long-time diffusion coefficient D_L. The diffusion inside the inner sphere of the depletion layer is the fastest and the diffusion of the outer sphere in the bulk is the slowest: $D_S > D_{S1} > D_L$. The depletion layer thickness $\delta = d + d_1$. All the three diffusive motions are assumed to be independent, so the MSD is the sum of the MSDs of both spheres and the probe:

$$\langle \boldsymbol{r}^2(t)\rangle = \langle \boldsymbol{r}_L{}^2(t)\rangle + \langle \boldsymbol{r}_{S1}{}^2(t)\rangle + \langle \boldsymbol{r}_S{}^2(t)\rangle \quad (2)$$

The exact MSD of the probe diffusing with the diffusion coefficient D inside a spherical domain of the radius d, with reflecting boundary conditions, is:[32]

$$\langle \boldsymbol{r}_S{}^2(t)\rangle = \frac{6d^2}{5} - 12d^2\sum_{n=1}^{\infty}\exp\left[-\beta_{1n}{}^2\frac{D_S t}{d^2}\right]\frac{1}{\beta_{1n}{}^2\left(\beta_{1n}{}^2-2\right)}, \quad (3)$$

where β_{1n} are the (non-zero) zeros of the derivatives of the spherical Bessel function, $j_1'(\beta_{1n}) = 0$. The first terms of (3) are:

$$\langle \boldsymbol{r}_S{}^2(t)\rangle = \frac{6}{5}d^2\left(1 - 0.99e^{-\frac{4.33D_S t}{d^2}} - 0.0085e^{-\frac{35.29D_S t}{d^2}} - \ldots\right) \quad (4)$$

As shown in our previous paper,[26] eqn (3) can be approximated by

$$\langle \boldsymbol{r}_S{}^2(t)\rangle = 6D_S\tau\left(1 - e^{-\frac{t}{\tau}}\right), \quad (5)$$

where $\tau = d^2/5D_S$ is the characteristic time of the motion within the inner shell. The total MSD (2) for the two spheres enclosed one in another is therefore:

$$\langle \boldsymbol{r}^2(t)\rangle = 6D_L t + \frac{6}{5}d_1{}^2\left(1 - e^{-\frac{5D_{S1}t}{d_1{}^2}}\right) + \frac{6}{5}d^2\left(1 - e^{-\frac{5D_S t}{d^2}}\right). \quad (6)$$

The characteristic time of the motion within the outer shell is $\tau_1 = d_1^2/(5D_{S1})$.

3 Methods

3.1 Experimental setup

For the DLS experiments we used a Spectra Physics Stabilite 2017 Argon ion laser, operated at the wavelength $\lambda = 514.5$ nm (delivering up to 2 W) and linearly polarized vertically. The scattered light was collected with a photon-counting PMT set on a BI-200SM goniometer (Brookhaven Instruments Corp.). We used the scattering angle $\theta = 90°$. The samples were held in a cell set in the center of a temperature-regulated cylindrical tank containing an index-matching liquid (decahydronaphthalene). The tank temperature was kept constant at 25 °C, with the accuracy of 0.01 °C, by means of a water bath. The autocorrelation function of the scattered light intensity was measured by processing the photocurrent using a PC-controlled 522-channel BI-9000 AT correlator. As samples, we used aqueous solutions of polyethylene glycol, PEG 600K and PEG 2M (purchased from Sigma Aldrich). The polydispersities of these polymers were previously measured (ref. 31) and are shown in Fig. 2 and Table 1. We used concentrations ranging from 0.3% to 2%. As probes, we used PS spheres of the radius $R = 20$ nm (Thermo Scientific) and $R = 43.5$ nm (Polysciences). We chose the concentrations of spheres such that their signal dominated over the signal from the polymer: in the solution volume of 1.5 ml, we used 10 μl of PS spheres for PEG 2M and $R = 20$ nm; 9 μl for PEG 600K and $R = 20$ nm; 6 μl for PEG 2M and $R = 43.5$ nm.

3.2 Fitting procedure

We fitted the autocorrelation function

$$g(q,t) = Ae^{-\frac{1}{3}q^2\langle r^2(t)\rangle} \quad (7)$$

where t is the time and $\boldsymbol{q} = 4\pi n\sin(\theta/2)/\lambda$ is the scattering wave vector. n is the index of refraction of the solution (here $n = 1.335$) (measured previously in ref. 31, SI Fig. 5). We used the MSD $\langle \boldsymbol{r}^2(t)\rangle$ given by eqn (1) to fit the single-shell model, and the MSD given by eqn (6) for the double-shell model. The experimental autocorrelation data have been cut off at the level of 0.05 because

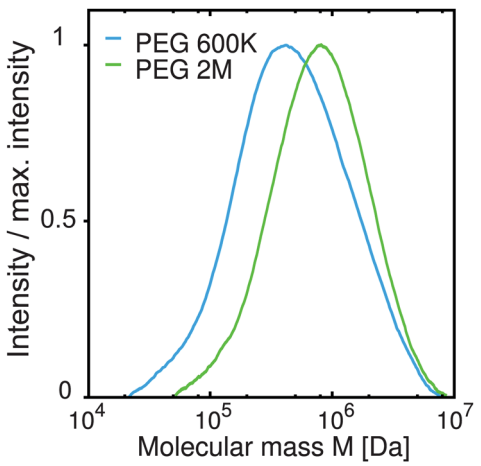

Fig. 2 The distribution of molecular masses for the commercially purchased PEG 600K and PEG 2M.[31] The polydispersity index is shown in Table 1.

at lower values (longer times) an additional relaxation time appeared which probably originated from long-time correlations in the polymer.[33] To plot the DLS autocorrelation data as the MSD, we transformed the formula (7):

$$\langle r^2(t)\rangle_{\text{data}} = -3\,\frac{\ln g(q,t)}{q^2}. \quad (8)$$

We first made an attempt to fit the single-shell model (1) to our experimental data. The fitting parameters were A, D_L, D_S, and d. The results are shown in Fig. 3A–C and Table 2. These results were not satisfactory because the model fitted the data for long time scales only.

We therefore fitted the double-shell model (6) to the data. The fitting parameters were A, D_L, D_S, d, and d_1. The fitting was done without weighting. We performed one measurement for each concentration because in the process of preparation of probes the dissolution of the polymer took a very long time. Table 1 contains the values of the fitted parameters and the fitting errors. To reduce the number of fitting parameters, we fixed the intermediate diffusion coefficient as $D_{S1} = D_L + (D_S - D_L)/8$, *i.e.* the value lying in the 1/8 between D_L and D_S. The choice of the division point was arbitrary: we tested setting the division point as one of the fitting parameters. We found that for PEG 2M, $R = 20$, the data for 0.5%, 0.75% and 1% converged to values close to 1/8. However, fitting the other data gave ambiguous results (convergence to different values depending on the changes in initial values) and introduced very large fitting errors. This indicated that the number of parameters was too large for correct fitting. For this reason, we fixed the division point at 1/8 for all data to eliminate these problems by decreasing the number of parameters and to make the results comparable between each other.

4 Results

We first tested the single-shell model (1) on our data. The results (Table 2) show that indeed it does not give satisfactory fits to the MSD of probes diffusing in PEG solutions (Fig. 3A–C). The model did not fit well in the short time scales, especially at larger PEG concentrations. The PEGs used in our experiments are flexible polymers and moreover they are strongly polydisperse (see Table 1 and ref. 31, SI Fig. 1). As in our previous study,[26] this fact suggests that the problems with fitting of the single-shell model to the diffusion in solutions of flexible and polydisperse polymers may be caused by the assumption that the depletion layer boundaries are perfectly reflecting. While it was sufficient for monodisperse, rigid polymers,[26] which can form a rigid cage around the probe, it turns out to be insufficient for description of the soft boundaries formed by flexible or polydisperse polymers.

We therefore fitted the double-shell model of depletion layer (eqn (6)) to the DLS measurements of motion of PS spheres in PEG solutions. Fig. 3D–F and Table 3 show the results of fitting. Since at times shorter than 5 μs the signal was dominated by noise, the double-shell model very well fits the data starting from ~5 μs up to 10^3 to 10^4 μs. The characteristic time scale τ of the motion inside the inner shell of the depletion layer is of the order of 10 μs, and the time scale τ_1 associated with the outer shell is of the order of 100 μs. We therefore conclude that the double-shell model of depletion layer very well describes diffusion of nanoparticles in PEG solutions.

Fig. 4A–C show that the thickness δ of the depletion layer decreases as the polymer concentration increases. However, the decrease of the inner shell thickness d is very weak, while the decrease of the outer shell thickness d_1 is strong.

We compared the fitted depletion layer thickness $\delta = d + d_1$ with the theoretical predictions of Fleer *et al.*[30] Their theoretical value of δ_{Fleer} was given by the formula:

$$\delta_{\text{Fleer}} = \left(R^3 + \frac{\pi^2\xi^2 {R_g}^2 R}{\pi\xi^2 + 4{R_g}^2} + \frac{6\xi R_g R^2}{\sqrt{\pi\xi^2 + 4{R_g}^2}} \right)^{1/3} - R, \quad (9)$$

where R is the radius of the spherical probe, R_g is the radius of gyration of the polymer, and ξ is the blob size of the polymer. We calculated the values of R_g and ξ using the following formulae: the phenomenological formula[34] for the radius of gyration is $R_g = 0.0215 M_n^{0.58}$ [nm], where M_n [g mol^{-1}] is the number average molecular mass of the polymer. The blob size ξ is a function of the polymer concentration c and of the radius of gyration:[35] $\xi = R_g(c^*/c)^{0.75}$ where c^* is the overlap concentration, defined for flexible polymers as $c^* = 3M_n/(4\pi R_g^3 N_A)$ (N_A is the Avogadro number). The values of these parameters are collected in Table 1 and the values of ξ for different PEG concentrations are shown in Table 3.

The depletion layer thickness $\delta = d + d_1$ determined in experiments is larger than the theoretical depletion layer thickness δ_{Fleer} (Fig. 4A–C; Table 3). δ_{Fleer} is closer to the thickness of the inner layer d. We note that δ_{Fleer}, similarly as d, d_1 and δ, decreases with increasing polymer concentration c. Thus, the theoretical formula (9) for the depletion layer thickness gives only a rough quantitative approximation of the inner (the most empty) region of the depletion layer, and it qualitatively reproduces the experimental dependence on the polymer concentration. The divergence from the predictions of Fleer *et al.* may be the result of strong polydispersity of the commercially purchased polymers (see Fig. 2 and Table 1).

Fig. 4D–F show the diffusion coefficients D_S, D_{S1}, and D_L depending on the thickness of the corresponding shells of the depletion layer model. The resulting profiles can be understood as approximations of the PEG density profiles around the probe. They are qualitatively similar to those predicted in earlier theoretical studies.[30,36] (We note that D_S and D_{S1} are the hypothetical diffusion coefficients inside the shells that move together with their content, and therefore the *observed* short time diffusion coefficients, which can be read out from the MSD plot in Fig. 3D–F, are the sum of $D_S + D_{S1} + D_L$.) We therefore conclude that the double-shell model allows approximation of the density profile around the probe.

5 Discussion

We have proposed a model that describes the effect of depletion layer on diffusion of nanoprobes in solutions of flexible and polydisperse polymers. Our double-shell model of walking confined diffusion approximates in a simple way the softness of the boundaries of the depletion layer: it divides the depletion layer around the probe into two regions. Our experiments with PEG solutions show that the inner region, which contains much less monomers than the bulk, has an almost

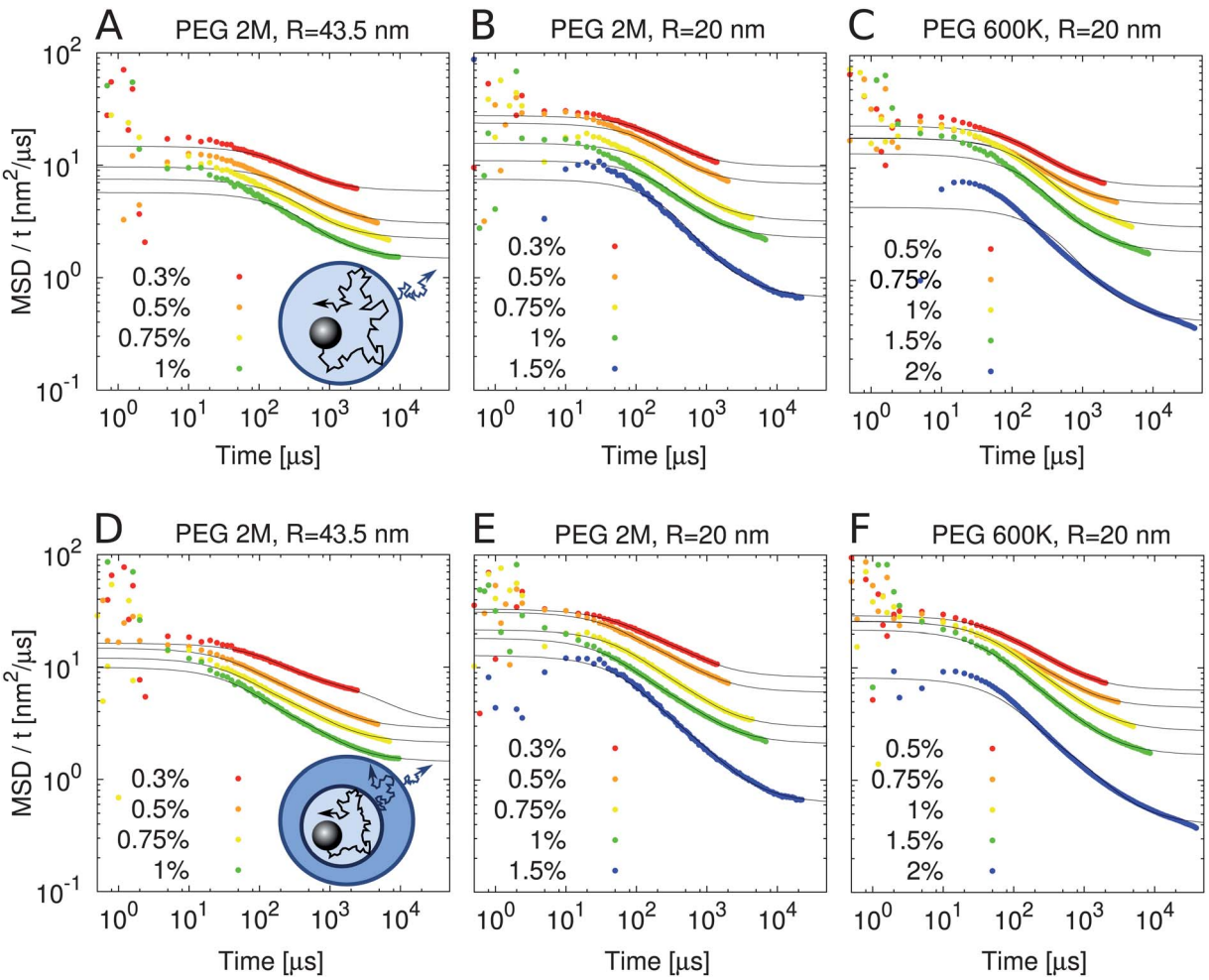

Fig. 3 The double-shell model of depletion layer describes the mean squared displacement of nanoparticles in PEG solutions better than the single-shell model. The single-shell model, eqn (1) (A–C), and the double-shell model, eqn (6) (D–F), were fitted to the DLS data for PS spheres of the radius R diffusing in aqueous solutions of PEG. (A and D) $R = 43.5$ nm, PEG 2M. (B and E) $R = 20$ nm, PEG 2M. (C and F) $R = 20$ nm, PEG 600 K. The fitted parameter values are shown in Tables 2 and 3. Dots represent the experimental results and solid lines represent the fits.

constant thickness d that only weakly decreases with increasing PEG concentration. On the other hand, the thickness d_1 of the outer region, where the polymer concentration is close to that in the bulk, decreases strongly with the PEG concentration.

Our model allows prediction of the depletion layer thickness, and it gives an approximate knowledge about the density profile around the probe. We note, however, that these predictions are made under particular assumptions: we assumed the empirical dissection into two arbitrarily chosen spheres, which imposes the

Table 2 The results of fitting of the single-shell model, eqn (1). The '±' values are the fitting errors

Polymer	R [nm]	c [%]	D_L [nm^2 μs^{-1}]	d [nm]	D_S [nm^2 μs^{-1}]	τ [μs]
PEG 2M	43.5	0.3	0.981 ± 0.008	32.0 ± 0.5	1.49 ± 0.04	138
	43.5	0.5	0.508 ± 0.005	32.5 ± 0.5	1.10 ± 0.03	193
	43.5	0.75	0.369 ± 0.003	28.6 ± 0.4	0.88 ± 0.04	185
	43.5	1	0.247 ± 0.002	26.8 ± 0.4	0.70 ± 0.04	203
PEG 2M	20	0.3	1.62 ± 0.03	41 ± 1	3.0 ± 0.1	114
	20	0.5	1.14 ± 0.01	39.8 ± 0.6	2.8 ± 0.1	112
	20	0.75	0.529 ± 0.007	37.8 ± 0.5	2.1 ± 0.1	136
	20	1	0.375 ± 0.005	32.7 ± 0.5	1.5 ± 0.1	146
	20	1.5	0.109 ± 0.001	31.2 ± 0.4	1.1 ± 0.1	170
PEG 600K	20	0.5	1.131 ± 0.009	38.5 ± 0.4	2.82 ± 0.05	105
	20	0.75	0.788 ± 0.007	35.6 ± 0.4	2.3 ± 0.1	111
	20	1	0.495 ± 0.005	37.5 ± 0.3	2.6 ± 0.1	108
	20	1.5	0.295 ± 0.003	33.4 ± 0.4	1.9 ± 0.1	115
	20	2	0.0705 ± 0.0008	27.8 ± 0.4	0.67 ± 0.05	231

Table 3 The results of fitting of the double-shell model, eqn (6). The diffusion coefficients in water were calculated using the formula: $D_{water} = k_B T/(6\pi\eta_0 R)$, where k_B is the Boltzmann constant, $T = 25$ °C is the temperature, $\eta_0 = 0.89$ cP is the viscosity of water, and R is the probe radius. The '±' values are the fitting errors

Polymer	R [nm]	R/R_g	c [%]	ξ [nm]	D_L [nm^2 μs^{-1}]	d_1 [nm]	D_{S1} [nm^2 μs^{-1}]	τ_1 [μs]	d [nm]	D_S [nm^2 μs^{-1}]	τ [μs]	$\delta = d + d_1$ [nm]	δ_{Fleer} [nm]	D_{water}/D_S	D_{water}/D_S
PEG 2M	43.5	0.98	0.3	37.0	0.53 ± 0.01	94 ± 7	0.7	2705	25.7 ± 0.8	1.54 ± 0.06	86	120 ± 7	27	4	11
			0.5	25.2	0.473 ± 0.004	34.4 ± 0.6	0.6	402	15.6 ± 0.5	1.4 ± 0.1	35	50.0 ± 0.7	21	4	12
			0.75	18.6	0.353 ± 0.003	28.8 ± 0.5	0.5	361	13.8 ± 0.6	1.2 ± 0.2	32	42.6 ± 0.8	16	5	16
			1	15.0	0.238 ± 0.002	26.2 ± 0.6	0.3	401	13.6 ± 0.8	1.1 ± 0.2	35	40 ± 1	14	5	24
PEG 2M	20	0.45	0.3	37.0	1.4 ± 0.1	50 ± 7	1.5	324	23 ± 2	2.6 ± 0.3	39	72 ± 8	24	5	9
			0.5	25.2	1.00 ± 0.03	43 ± 2	1.2	294	22.6 ± 0.6	2.9 ± 0.2	35	65 ± 2	19	4	12
			0.75	18.6	0.49 ± 0.01	36 ± 1	0.7	358	23.6 ± 0.7	2.4 ± 0.2	46	60 ± 1	15	5	25
			1	15.0	0.348 ± 0.005	32.2 ± 0.8	0.6	363	18.7 ± 0.8	2.1 ± 0.3	33	51 ± 1	13	6	35
			1.5	11.1	0.103 ± 0.001	27.8 ± 0.8	0.3	506	20.1 ± 0.8	1.7 ± 0.2	47	48 ± 1	10	7	119
PEG 600K	20	0.65	0.5	24.8	1.048 ± 0.009	38.0 ± 0.6	1.2	233	22.0 ± 0.3	2.56 ± 0.09	38	60.0 ± 0.7	17	5	12
			0.75	18.3	0.734 ± 0.006	35.1 ± 0.5	1.0	254	20.1 ± 0.3	2.6 ± 0.2	31	55.2 ± 0.6	14	5	17
			1	14.8	0.455 ± 0.004	34.3 ± 0.8	0.8	300	24.5 ± 0.3	3.1 ± 0.1	39	58.8 ± 0.6	12	4	27
			1.5	10.9	0.277 ± 0.003	30.3 ± 0.8	0.6	312	21.3 ± 0.7	2.8 ± 0.3	33	52 ± 1	10	4	44
			2	8.8	0.0662 ± 0.0006	26.4 ± 0.6	0.2	715	16.8 ± 0.7	1.1 ± 0.1	52	43.2 ± 0.9	8	11	185

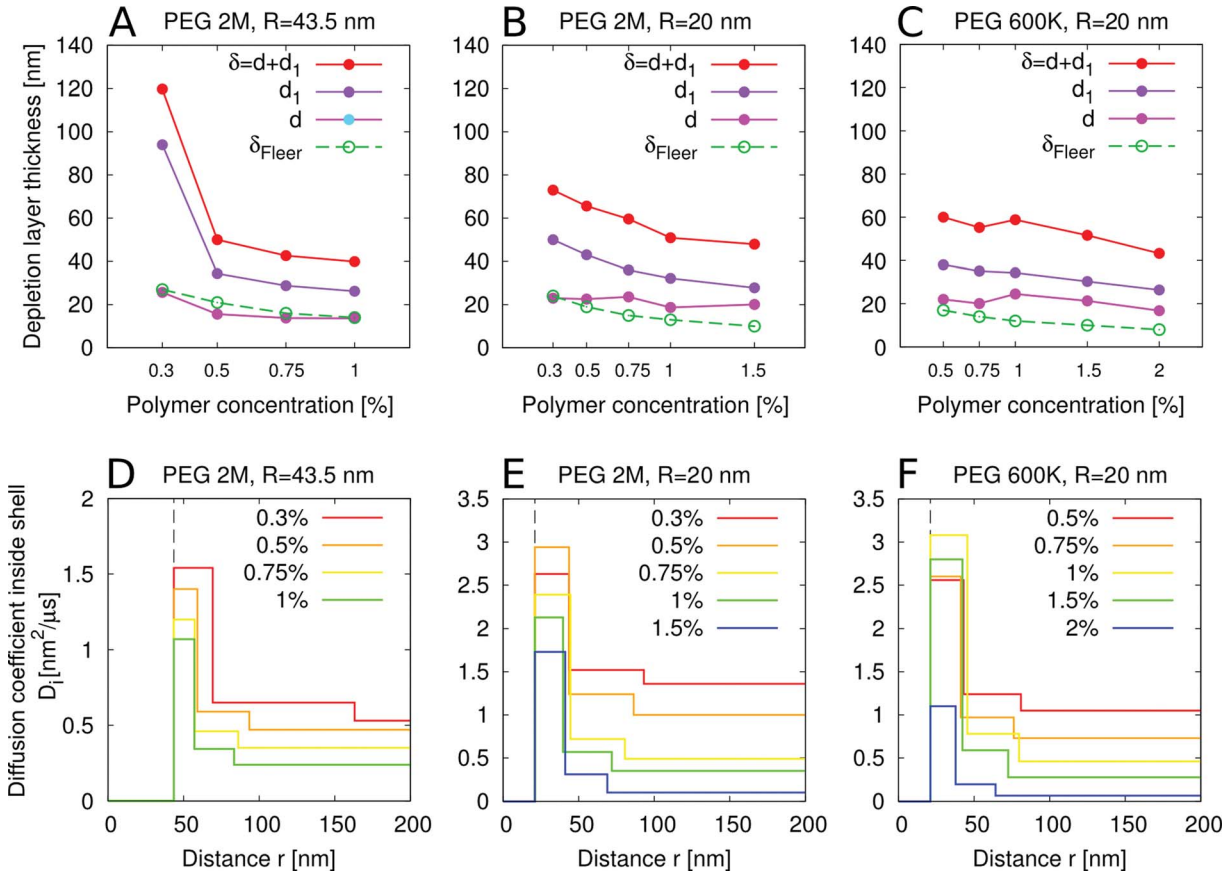

Fig. 4 The double-shell model predicts the depletion layer thickness and allows approximation of the density profile around the probe. (A–C) The thickness d of the inner shell, the thickness d_1 of the outer shell, and the total depletion layer thickness $\delta = d + d_1$ are compared with the theoretical depletion layer thickness δ_{Fleer} calculated using the formula (9) of Fleer *et al.*[30] The depletion layer thickness decreases as the polymer concentration increases, however the inner shell thickness remains almost unaffected. (D–F) The diffusion coefficient D_i inside the shell, depending on the thickness of the corresponding shells. Note that since the shells move together with their content, the observed diffusion coefficients D, which can be read out from the MSD plot in Fig. 3, are the sums of the diffusion coefficients in subsequent shells. For the motion of the probe within the inner layer, $D_i = D_S$ and $D = D_S + D_{S1} + D_L$. For motion of the probe and the inner layer within the outer layer, $D_i = D_{S1}$ and $D = D_{S1} + D_L$. For the motion of the probe and both layers in the bulk, $D_i = D = D_L$. In order to compare the thicknesses with the probe size, the distance r on the plot is measured from the center of the probe. The resulting profiles can be understood as approximations of the polymer density profiles around the probe.

assumption that the model polymers are much less polydisperse than the experimental probe is; the spheres are assumed to be independent; and the exponential form of eqn (5) for MSD is an approximation.

On the other hand, the previous theories attempting to predict the depletion layer thickness give results that are complementary to our model: the theory of Fleer *et al.*[30] approximately reproduces the thickness d of the inner shell of the depletion layer (Fig. 4A–C; Table 3). The divergence between our results and the predictions of Fleer *et al.* may be caused by strong polydispersity of the commercially purchased polymers. Then again, the single-shell model[26] (1) fits the intermediate and long time scales only, so the fitted depletion layer thickness in that model, which is similar to d_1, can be interpreted as detection of the motion of the probe together with the inner regions of the depletion layer. Thus, the single-shell model approximately reproduces the outer shell thickness d_1 (Table 2).

The presence of depletion layer around diffusing particles may have deep consequences for rotational diffusion. Kuttner *et al.*[37] separately measured the contributions of translational and rotational diffusion to association kinetics of proteins in solutions of PEG 8000. They found that while the translational diffusion constantly slowed down with increasing PEG concentration, the rotational diffusion in PEG did not become slower than a certain level (1/4 of the rotational diffusion coefficient in water). A similar result was obtained with Brownian dynamics simulations of diffusion of proteins in eukaryotic cytoplasm: McGuffee *et al.*[38] found that the rotational diffusion coefficient in cytoplasm was ~1/3 of that in water while the translational diffusion coefficient was ~1/10 of that in water. We hypothesize that the different scaling of the rotational and translational diffusion coefficients may be caused by the presence of depletion layer, since the concentration of crowding agents in its inner region is much lower than in the bulk solution. In our present study, we found that the translational diffusion coefficient D_S in the inner region of the depletion layer is 1/11 − 1/4 of that in water. At the same time, the long-time translational diffusion coefficient D_L is 1/185 − 1/9 of that in water (Table 3). Therefore, we propose a hypothesis that the rotational diffusion should scale as D_S rather than as D_L.

The effect of depletion layer on rotational diffusion may be especially important in calculating the rates of biochemical reactions in the crowded environment inside living cells. Understanding how the macromolecular crowding differently affects translational and rotational diffusion is necessary to correctly calculate the search times for DNA sites by transcription factors[39] or repair proteins:[40,41] the existing calculations[39–41] assume that rotational diffusion scales in the same way as translational diffusion, which may lead to incorrect results.

We thus argue that, based on the predictions of thickness of the depletion layer and the structure of its boundaries, one may attempt to predict the consequences of this effect, such as increased rotational diffusion and changes in rates of biochemical reactions.

Acknowledgements

The project was supported from the budget of the National Science Center within the projects: DEC-2011/02/A/ST3/00143 (MAESTRO grant – R.H.) and 2011/01/D/ST3/00751 (SONATA grant – A.O.M.).

References

1 M. J. Skaug, R. Faller and M. L. Longo, *J. Chem. Phys.*, 2011, **134**, 215101.
2 R. Tero, G. Sazaki, T. Ujihara and T. Urisu, *Langmuir*, 2011.
3 E. Vilaseca, I. Pastor, A. Isvoran, S. Madurga, J. L. Garcés and F. Mas, Theoretical chemistry accounts: theory, computation, and modeling, *Theor. Chim. Acta*, 2011, **128**, 795–805.
4 A. Kusumi, C. Nakada, K. Ritchie, K. Murase, K. Suzuki, H. Murakoshi, R. S. Kasai, J. Kondo and T. Fujiwara, *Annu. Rev. Biophys. Biomol. Struct.*, 2005, **34**, 351–378.
5 M. J. Saxton and K. Jacobson, *Annu. Rev. Biophys. Biomol. Struct.*, 1997, **26**, 373–399.
6 M. R. Horton, F. Höfling, J. Rädler and T. Franosch, *Soft Matter*, 2010, **6**, 2648–2656.
7 A. Kammerer, F. Höfling and T. Franosch, *EPL*, 2008, **84**, 66002.
8 F. Höfling and T. Franosch, *Phys. Rev. Lett.*, 2007, **98**, 140601.
9 I. Golding and E. C. Cox, *Phys. Rev. Lett.*, 2006, **96**, 98102.
10 M. Weiss, M. Elsner, F. Kartberg and T. Nilsson, *Biophys. J.*, 2004, **87**, 3518–3524.
11 I. Sokolov, *Soft Matter*, 2012, DOI: 10.1039/c2sm25701g.
12 M. Saxton, *Biophys. J.*, 1996, **70**, 1250–1262.
13 F. Santamaria, S. Wils, E. De Schutter and G. Augustine, *Eur. J. Neurosci.*, 2011, **34**(4), 561–568.
14 F. Santamaria, S. Wils, E. De Schutter and G. Augustine, *Neuron*, 2006, **52**, 635–648.
15 M. Saxton, *Biophys. J.*, 2007, **92**, 1178–1191.
16 M. Platani, I. Goldberg, A. Lamond and J. Swedlow, *et al.*, *Nat. Cell Biol.*, 2002, **4**, 502–508.
17 R. Metzler, B. Broek, G. Wuite and M. Lomholt, *Biophysics of DNA-Protein Interactions*, 2011, pp. 69–84.
18 M. Lomholt, B. Van Den Broek, S. Kalisch, G. Wuite and R. Metzler, *Proc. Natl. Acad. Sci. U. S. A.*, 2009, **106**, 8204.
19 F. Höfling, K. Bamberg and T. Franosch, *Soft Matter*, 2011, **7**, 1358–1363.
20 L. Wawrezinieck, H. Rigneault, D. Marguet and P. Lenne, *Biophys. J.*, 2005, **89**, 4029–4042.
21 I. Goychuk, *Phys. Rev. E: Stat., Nonlinear, Soft Matter Phys.*, 2009, **80**, 046125.
22 M. Lee, S. Cardinali, D. Reich, K. Stebe and R. Leheny, *Soft Matter*, 2011, **7**, 7635–7642.
23 M. Saxton, *Biophys. J.*, 2001, **81**, 2226–2240.
24 R. Hanes, C. Dalle-Ferrier, M. Schmiedeberg, M. Jenkins and S. Egelhaaf, *Soft Matter*, 2012, **8**, 2714–2723.
25 K. Kremer, in *Computational Soft Matter: From Synthetic Polymers to Proteins, Lecture Notes*, ed. N. Attig, K. Binder, H. Grubmüller and K. Kremer, John von Neumann Institute for Computing, Jülich, 2004, vol. 23, Entangled polymers: From universal aspects to structure property relations, pp. 141–168.
26 A. Ochab-Marcinek and R. Hołyst, *Soft Matter*, 2011, **7**, 7366–7374.
27 S. Asakura and F. Oosawa, *J. Polym. Sci.*, 1958, **33**, 183–192.
28 A. Vrij, *Pure Appl. Chem.*, 1976, **48**, 471–483.
29 P. G. de Gennes, *Scaling Concepts in Polymer Physics*, Cornell Univ. Pr, 1979.
30 G. J. Fleer, A. M. Skvortsov and R. Tuinier, *Macromolecules*, 2003, **36**, 7857–7872.
31 N. Ziębacz, S. A. Wieczorek, T. Kalwarczyk, M. Fiałkowski and R. Hołyst, *Soft Matter*, 2011, **7**, 7181.
32 T. Bickel, *Phys. A*, 2007, **377**, 24–32.
33 S. A. Wieczorek, E. Freyssingeas and R. Holyst, *J. Phys. Chem. B*, 2005, **109**, 16252–16262.
34 K. Devanand and J. C. Selser, *Macromolecules*, 1991, **24**, 5943–5947.
35 T. Kalwarczyk, N. Ziębacz, A. Bielejewska, E. Zaboklicka, K. Koynov, J. Szymanski, A. Wilk, A. Patkowski, J. Gapinski, H. Butt and R. Hołyst, *Nano Lett.*, 2011, **11**, 2157.
36 R. Tuinier and H. N. W. Lekkerkerker, *Macromolecules*, 2002, **35**, 3312–3313.
37 Y. Y. Kuttner, N. Kozer, E. Segal, G. Schreiber and G. Haran, *J. Am. Chem. Soc.*, 2005, **127**, 15138–15144.
38 S. R. McGuffee and A. H. Elcock, *PLoS Comput. Biol.*, 2010, **6**, e1000694.
39 G. W. Li and J. Elf, *FEBS Lett.*, 2009, **583**, 3979–3983.
40 P. C. Blainey, A. M. Van Oijen, A. Banerjee, G. L. Verdine and X. S. Xie, *Proc. Natl. Acad. Sci. U. S. A.*, 2006, **103**, 5752–5757.
41 P. C. Blainey, G. Luo, S. C. Kou, W. F. Mangel, G. L. Verdine, B. Bagchi and X. S. Xie, *Nat. Struct. Mol. Biol.*, 2009, **16**, 1224–1229.